Journal of
Synchrotron Radiation

ISSN 0909-0495

Received 12 May 2005
Accepted 17 November 2005

Coherent propagation of white X-rays in a planar waveguide

Christian Fuhse,* Christoph Ollinger, Sebastian Kalbfleisch and Tim Salditt

Institut für Röntgenphysik, Universität Göttingen, Friedrich-Hund-Platz 1, 37077 Göttingen, Germany. E-mail: cfuhse@uni-goettingen.de

The far-field diffraction pattern of a front-coupled planar waveguide supporting two guided modes has been measured using a white X-ray beam. Interference of the guided modes leads to a characteristic variation of the far-field diffraction pattern for different photon energies. The experiment verifies the predicted properties of the guided modes, shows that these modes superpose coherently, and demonstrates that the electromagnetic field downstream of the waveguide is significantly different from that expected for a hypothetical small slit of the same size.

Keywords: X-ray waveguides; front-coupling.

1. Introduction

X-ray waveguides are promising optical elements that may act as very small sources providing highly coherent and slightly divergent beams. X-rays may be confined in one (Spiller & Segmüller, 1973) or two (Pfeiffer *et al.*, 2002) dimensions to a small guiding core surrounded by a cladding material with lower refractive index and typically significantly higher absorption. Depending on the utilized materials, the cross-section dimensions of the guiding core may be as low as approximately 10 nm (Bergemann *et al.*, 2003).

For potential applications, *e.g.* in coherent X-ray imaging (Lagomarsino *et al.*, 1997) and scattering (Jark *et al.*, 2000), it is crucial to obtain both high flux and low background in the exiting beam. These requirements are met by a waveguide situated in the focus of a pre-focusing device where the X-ray beam is directly coupled into the front side of the waveguide (Fuhse *et al.*, 2004; Jarre *et al.*, 2005). The high density of flux provided by the pre-focusing device is thus combined with the smaller cross-section dimensions and better background suppression of the waveguide. In contrary to other common coupling techniques like resonant beam coupling (Feng *et al.*, 1993; Jarre *et al.*, 2004) or coupling *via* a standing wave above the substrate (Zwanenburg *et al.*, 1999), this technique does not allow for a selective excitation of individual modes in a multimodal waveguide. The electromagnetic field in a multimodal waveguide is thus rather given as a superposition of multiple guided modes propagating with their individual propagation constants. Assuming a coherent incident X-ray beam, the individual modes interfere coherently and the electromagnetic field inside the guiding core consists of a quite complex interference pattern (Fuhse & Salditt, 2005). Although it seems not feasible to measure the electromagnetic field distribution directly, the field distribution at the exit of a waveguide may be deduced from the far-field diffraction pattern.

In addition to these fundamental aspects of X-ray wave propagation in confined geometry which can conveniently be addressed by considering the energy dependence of the far-field diffraction pattern, the presence of a white beam is also motivated by possible improvements for future experiments. Increasing the energy bandwidth (*e.g.* using a full undulator harmonic) can boost the number of photons available for experiments. This advantage is obvious for fluorescence spectroscopy, but also in phase-contrast imaging the monochromaticity can be relaxed in many cases. Therefore it is important to investigate the simultaneous propagation of different photon energies in the same waveguide.

In the present experiment a planar waveguide supporting two guided modes is illuminated by an unfocused collimated white X-ray beam. The far-field diffraction patterns corresponding to different photon energies are simultaneously measured using an energy-dispersive semiconductor detector. The shape of the far-field diffraction pattern basically depends on the phase difference between the two guided modes at the exit of the waveguide. The dependence of this phase difference on the photon energy leads to a characteristic variation of the far-field diffraction pattern for different energies which confirms the coherent propagation of two guided modes and allows for an experimental verification of calculated individual propagation constants.

2. Mode propagation in planar X-ray waveguides

The electromagnetic field inside an X-ray waveguide is adequately described by the Helmholtz equation,

$$\nabla^2\psi + n^2k^2\psi = 0,$$

where ψ denotes the scalar wavefield, ∇^2 denotes the Laplacian, $n = 1 - \delta - ib$ denotes the refractive index, and k is the wavenumber in free space. Each planar waveguide supports a finite number of guided modes. For symmetric waveguides, *i.e.* waveguides where the cladding material on both sides is the same, the number of guided modes is given by (Marcuse, 1974)

$$N = [V/\pi]_{\rm int}.$$

The symbol $[\,]_{\rm int}$ indicates the next larger integer from the value in the brackets, and the dimensionless waveguide parameter V is given by

$$V = \left(n_1^2 - n_2^2\right)^{1/2} kd \simeq (2\delta_2 - 2\delta_1)^{1/2} kd.$$

Here, n_1 denotes the refractive index of the guiding layer, n_2 denotes the index of the cladding, and d is the thickness of the guiding layer. Away from the absorption edges, the dispersive part of the refractive index is given by (Als-Nielsen, 2001)

$$\delta = 2\pi r_{\rm e}\,\rho/k^2,$$

where $r_{\rm e}$ is the classical electron radius, $\sim 2.82 \times 10^{-15}$ m, and ρ is the electron density. With $\Delta\rho = \rho_2 - \rho_1$ we find

$$V = 2(\pi r_{\rm e}\,\Delta\rho)^{1/2} d.$$

Accordingly, the number of guided modes does not depend on the energy of the X-rays. Sufficiently far away from the entrance, the scalar wavefield inside the waveguide is given as a linear combination of guided modes (Marcuse, 1974),

$$\psi(x, z) = \sum_{\rm m} c_{\rm m}\psi_{\rm m}(z)\exp(-i\beta_{\rm m}x)$$

with

$$\psi_{\rm m}(z) = \begin{cases} \exp(\gamma_{\rm m}z) & \text{if} \quad z < 0 \\ \cos(\kappa_{\rm m}z) + (\gamma_{\rm m}/\kappa_{\rm m})\sin(\kappa_{\rm m}z) & \text{if} \quad 0 \le z \le d \\ [\cos(\kappa_{\rm m}d) + (\gamma_{\rm m}/\kappa_{\rm m})\sin(\kappa_{\rm m}d)] \times \exp[-\gamma_{\rm m}(z - d)] & \text{if} \quad z > d \end{cases}$$

The propagation constants $\beta_{\rm m}$ as well as the constants $\kappa_{\rm m}$ and $\gamma_{\rm m}$ have to be determined numerically by solving the corresponding transcendental eigenvalue equation (Marcuse, 1974). However, the values of $\kappa_{\rm m}d$ and $\gamma_{\rm m}d$ are uniquely determined by V (Marcuse, 1974; Yeh, 1990). Since V is independent of the photon energy, this also applies to $\kappa_{\rm m}$ and $\gamma_{\rm m}$. The coefficients $c_{\rm m}$ are given by the projection of the incident field $\psi_{\rm in}$ onto the respective eigen modes (Bongaerts *et al.*, 2002),

$$c_{\rm m} = ||\psi_{\rm m}||^{-2} \int \psi_{\rm in}(z)\,\psi_{\rm m}(z)\,{\rm d}z. \qquad (1)$$

For an incident plane wave the coefficients $c_{\rm m}$ depend on the angle of incidence $\alpha_{\rm i}$. The waveguide measured in this work supports two guided modes ψ_0 and ψ_1. An incident plane wave may thus excite these two modes propagating through the waveguide with their individual propagation constants β_0 and β_1. As illustrated in Fig. 1, the differences in the propagation constants lead to the formation of a characteristic interference pattern inside the waveguide (Fuhse & Salditt, 2005). In particular, the shape of the electric field at the exit of the waveguide depends on the phase difference between the individual modes. This phase difference is

$$\Delta\varphi_{01} = (\beta_0 - \beta_1)\ell,$$

where ℓ is the length of the waveguide. According to Marcuse (1974) we have $\beta_{\rm m}^2 = n_1^2k^2 - \kappa_{\rm m}^2$. Since $n_1k \gg \kappa_{\rm m}$ we approximate $\beta_{\rm m} \simeq n_1k - \kappa_{\rm m}^2/2n_1k$ and with $n_1 \simeq 1$ we find

$$\beta_0 - \beta_1 \simeq \left(\kappa_1^2 - \kappa_0^2\right)/2k.$$

As mentioned above, $\kappa_{\rm m}$ does not depend on k. Hence, the difference between the propagation constants as well as the phase difference at the exit of the waveguide is inversely proportional to k or the photon energy E.

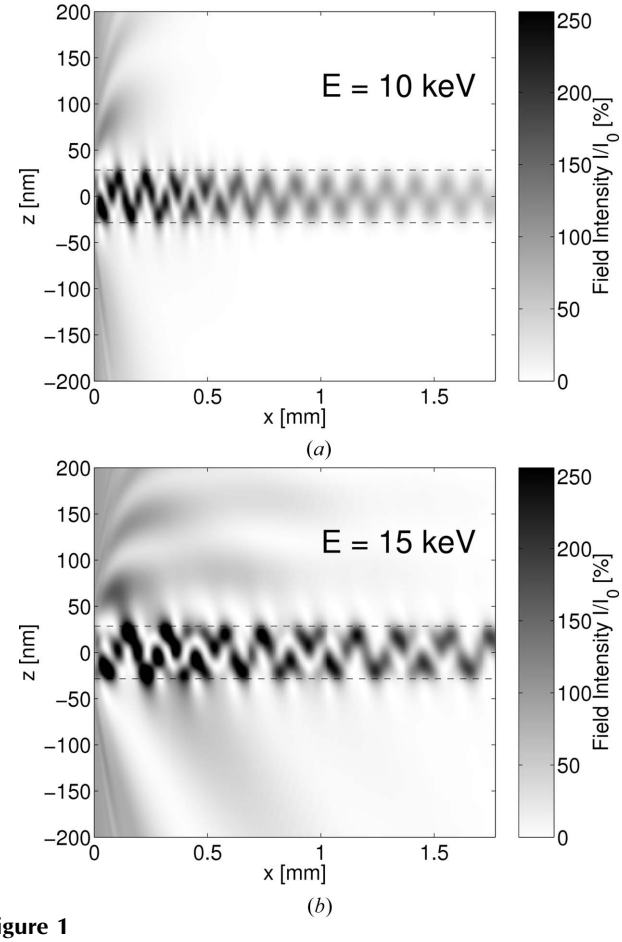

Figure 1
The electromagnetic field intensity pattern inside a polymer (calixarene) waveguide of thickness d = 57 nm in Si was calculated using a Crank–Nicolson-like finite-difference scheme (Scarmozzino & Osgood, 1991) solving the parabolic wave equation (Kopylov *et al.*, 1995). The X-ray beams with E = 10 keV and E = 15 keV, respectively, arrive from above left with an angle of incidence $\alpha_{\rm i} = 0.03°$. The dashed lines indicate the interfaces between the guiding layer and the cladding. The calculations show how the interference pattern inside the waveguide is stretched in the propagation direction with increasing photon energy. Furthermore, owing to the lower absorption at higher energies, a standing wave corresponding to the specularly reflected beam is visible in the cladding above the guiding layer at E = 15 keV.

Experimentally, the electromagnetic field at the exit of the waveguide may be deduced from the measured far-field diffraction pattern. The latter can be described using the Fraunhofer diffraction formalism given in the small-angle approximation as

$$I(k_f) = I_0 \left| \int \psi(\ell, z) \exp\left(ik_f z\right) \mathrm{d}z \right|^2, \qquad (2)$$

where $k_f = k \sin\alpha_f$ is the z component of the wavevector (Fig. 2). Neglecting absorption, we find

$$I(k_f) = I_0 \left| c_0 \tilde{\psi}_0(k_f) + c_1 \exp\left[-i\left(\beta_1 - \beta_0\right)\ell\right] \tilde{\psi}_1(k_f) \right|^2,$$

where the tilde denotes the Fourier transform. Assuming that the coefficients c_m do not strongly depend on the X-ray energy, the far-field diffraction pattern (measured as a function of k_f) is approximately the same for each two energies where the difference in $\Delta\varphi_{01}$ is an integer multiple of 2π. Since $\Delta\varphi_{01}$ scales with E^{-1}, the far-field diffraction pattern is periodic in E^{-1} with a period

$$\Delta_{E^{-1}} = 8\pi^2 / \left[\left(\kappa_1^2 - \kappa_0^2\right)\ell hc\right]. \qquad (3)$$

Here, h is Planck's constant and c is the speed of light. Since the values of $\kappa_0 d$ and $\kappa_1 d$ are uniquely determined by V, the period $\Delta_{E^{-1}}$ only depends on V, d and ℓ.

Depending on the phase difference between the guided modes at the exit of the waveguide, the maximum of the far-field intensity distribution oscillates between positive and negative exit angles α_f unless α_i is exactly zero. Accordingly, the spectrum measured at a fixed exit angle shows characteristic oscillations with photon energy E.

3. Experiment

The experiment was carried out at the energy-dispersive reflectometry (EDR) white-beam dipole beamline at BESSY II (Panzner *et al.*, 2003). The dimensions of the incident beam were defined by horizontal and vertical slits to 200 µm × 20 µm. The Si drift chamber detector (Röntec XFlash 1000) has an energy resolution of approximately 200 eV and was placed 1.04 m away from the waveguide. The detector aperture was 50 µm in the vertical direction, corresponding to an angular resolution of $\sim 0.003^\circ$ in 2θ (Fig. 2).

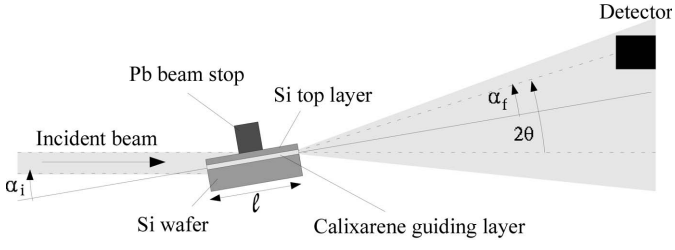

Figure 2
Experimental set-up. The X-ray beam is coupled directly onto the front side of the waveguide. The intensity distribution in the far-field is measured for different incident angles α_i. Depending on the photon energy, the maximum of the intensity pattern is found above or below $\alpha_\mathrm{f} = 0$. (Distances and angles are not to scale.)

The X-ray waveguide consists of a planar thin-film structure on a standard Si wafer with an organic guiding layer (calixarene) and a Si cladding. The thickness of the spin-coated calixarene layer (Allresist XAR-N7600/2) was determined to 57 nm by X-ray reflectivity. The upper Si cladding was deposited by electron beam evaporation (Univex 450, Leybold) and has a thickness of approximately 200 nm. Atop the waveguide structure a piece of lead tape was fixed with silver dag (Conrad Silberleitlack) to block out the remaining part of the primary beam.

We have measured two samples of the same waveguide structure with lengths ℓ of 1.77 ± 0.05 mm and 4.1 ± 0.1 mm,

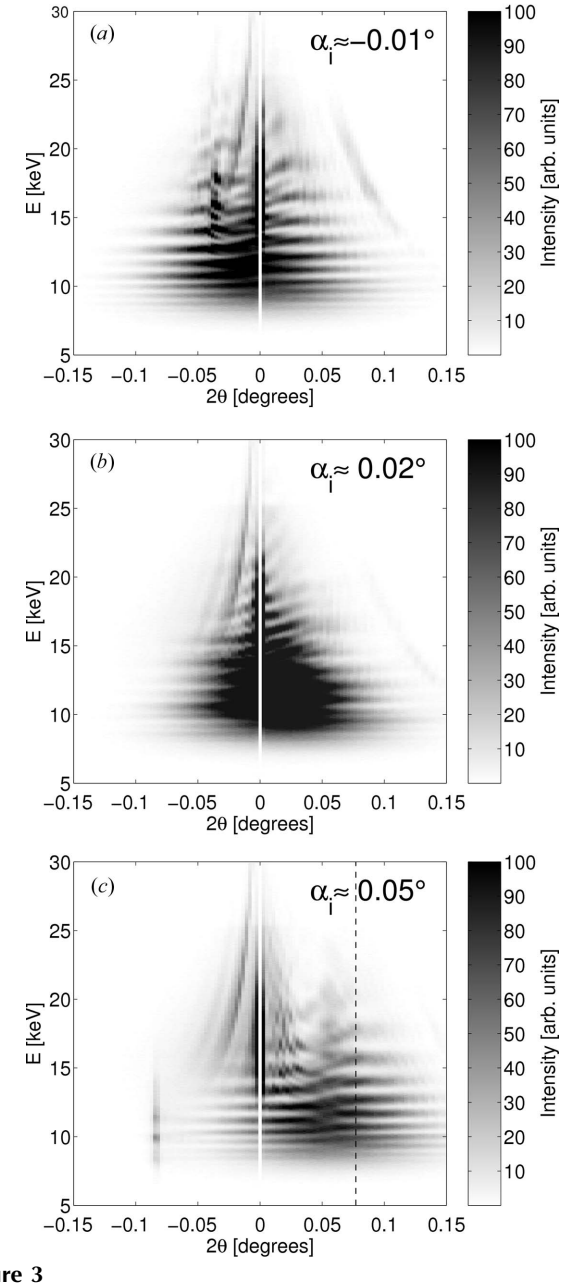

Figure 3
Far-field diffraction patterns measured behind the short waveguide ($\ell \simeq 1.8$ mm) at different incident angles α_i. For $2\theta = 0$, no spectra could be measured owing to the high intensity of the transmitted beam. The dashed line in (*c*) indicates the spectrum plotted in Fig. 5(*a*).

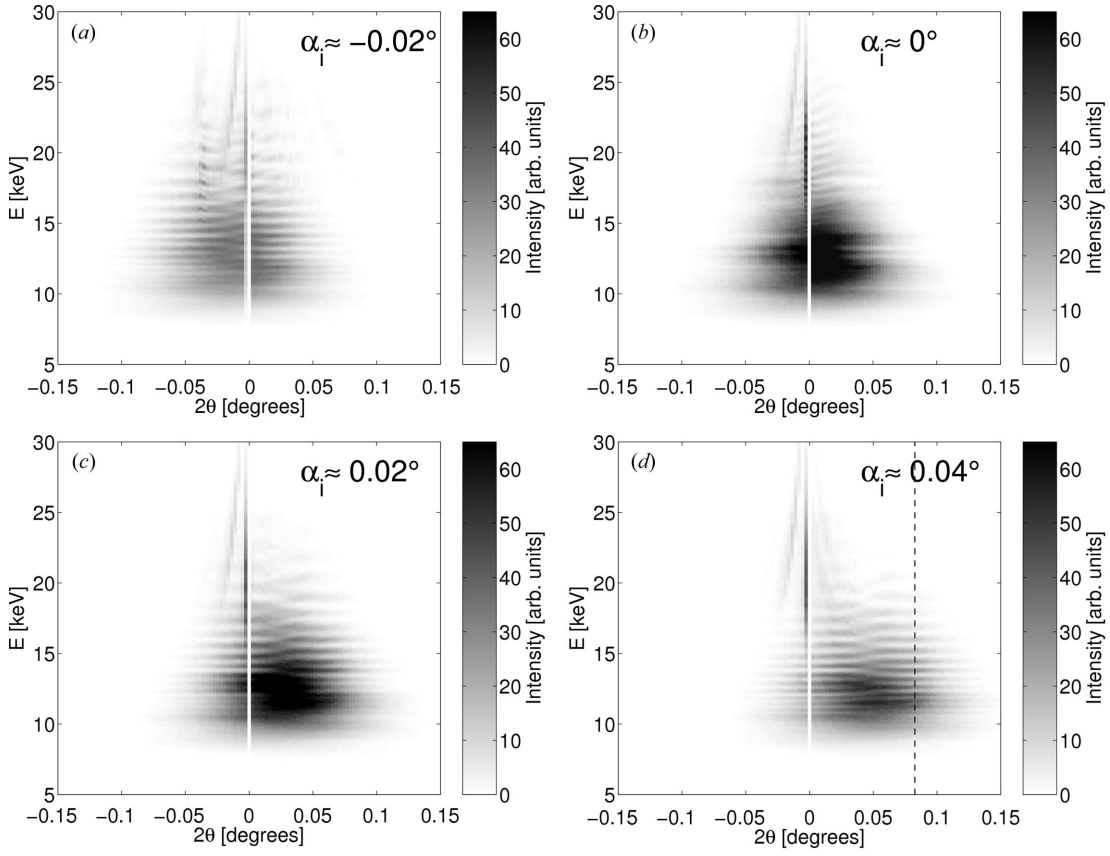

Figure 4
Far-field diffraction patterns measured behind the long waveguide ($\ell \simeq 4.1$ mm). For $2\theta = 0$, no spectra could be measured owing to the high intensity of the transmitted beam. The dashed line in (*d*) indicates the spectrum plotted in Fig. 5(*b*).

respectively. Assuming densities of 2.33 g cm^{-3} for Si and 1.18 g cm^{-3} for calixarene ($C_{60}H_{60}O_{12}$), we find $V \simeq 2\pi$ and thus the waveguide supports two guided modes.[1] The corresponding mode constants are $\kappa_0 d \simeq 2.37$ and $\kappa_1 d \simeq 4.63$.

Figs. 3 and 4 show far-field diffraction patterns measured for different angles of incidence α_i. The angle of incidence was increased in steps of 0.03° and 0.02°, respectively. The absolute values of α_i are estimated from the centers of the diffraction patterns expected at $2\theta = -\alpha_i$. Alternatively, the absolute values could be derived from the positions of the specularly reflected beams visible in Figs. 3(*a*) and 4(*a*). However, this gives slightly different values which is probably due to interference of the reflected beam with the waveguide far-field.

For low energies there is no intensity transmitted due to strong absorption in both the Si and the guiding layer. For medium energies between ∼10 keV and ∼15 keV we obtain a nearly undisturbed waveguide far-field in agreement with the expression given in equation (2). The center of the diffraction pattern moves in 2θ with α_i, and the total intensity decreases with increasing $|\alpha_i|$. Along the energy axis the angular position of the maximum oscillates between positive and negative α_f values. These oscillations are also clearly visible in spectra measured at fixed exit angles as shown in Fig. 5. Plotted over E^{-1}, these spectra yield periods of 3.22×10^{-3} keV^{-1} for the short waveguide and 7.48×10^{-3} keV^{-1} for the longer one. From equation (3) we expect $\Delta_{E^{-1}} = (3.2 \pm 0.1) \times 10^{-3}$ keV^{-1} and $\Delta_{E^{-1}} = (7.4 \pm 0.2) \times 10^{-3}$ keV^{-1}, respectively, in agreement with the experimental results. When α_i is very close to zero, these oscillations are hardly visible. This is due to the fact that for $\alpha_i = 0$ the overlap integral in equation (1) vanishes for all odd modes and thus the ψ_1 mode is not excited. Accordingly, the far-field diffraction pattern measured for very small $|\alpha_i|$ is a slightly disturbed pattern of the ψ_0 mode.

At very high energies the absorption of the Si cladding decreases significantly and the waveguide far-field is superposed by transmitted and specularly reflected beams, accompanied by other disturbing contributions that are probably related to diffraction of these beams. The intense high-energy components in the transmitted beam also made it impossible to measure spectra at $2\theta = 0$. Note that the Si cladding is almost transparent for the high energies (for the short waveguide, already at $E = 15$ keV the transmission is 2%). But since the width of the transmitted beam is much smaller than the width of the waveguide far-field, only one line is missing in the patterns shown in Figs. 3 and 4. However, the intensity of the

[1] The exact value $V \simeq 6.294$, which is slightly larger than 2π, implies that there are three guided modes. However, in this case the ψ_2 mode is very close to cut-off. Consequently, a large portion of power is transmitted in the cladding and the ψ_2 mode is subject to significantly higher absorption than the other guided modes. Furthermore, for small α_i, the value of the overlap integral in equation (1) is very small. So we may neglect the ψ_2 contributions.

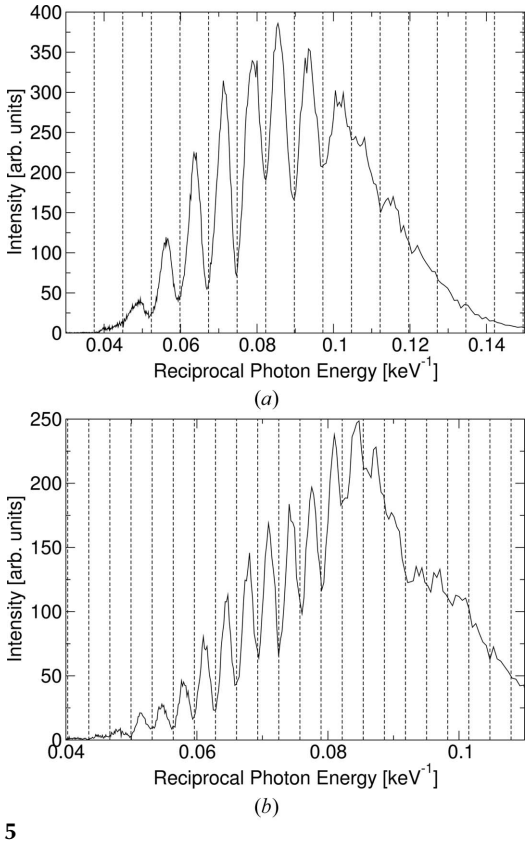

Figure 5
The spectra measured at a fixed exit angle α_f in the far-fields of the short (*a*) and long (*b*) waveguide show characteristic oscillations that are equidistantly spaced in E^{-1}. This spacing decreases with an increasing waveguide length. A local maximum in the spectrum corresponds to an energy for which the maximum of the far-field diffraction pattern appears at $\alpha_f > 0$, while local minima in the spectrum correspond to energies for which the maximum of the far-field diffraction pattern appears at $\alpha_f < 0$. As indicated by the dashed lines, the measurements yield periods of $\Delta_{E^{-1}} = 7.48 \times 10^{-3}\,\mathrm{keV}^{-1}$ (*a*) and $\Delta_{E^{-1}} = 3.22 \times 10^{-3}\,\mathrm{keV}^{-1}$ (*b*), respectively.

waveguided beam itself decreases corresponding to a decrease in the spectrum of the bending magnet (Panzner *et al.*, 2003).

Apart from verifying the theory of mode propagation, the experiment also shows the energy range within which the waveguide is suited for applications. At the lower end, significant absorption in the waveguide damps the far-field intensity, while at the upper end the far-field diffraction pattern is disturbed by radiation transmitted through the cladding. Since both ends are determined by absorption, the applicative energy range can be adapted to higher or lower energies by increasing or decreasing the length of the waveguide. Note that the shorter waveguide provides significantly higher intensity particularly for lower energies near 10 keV, while the far-field of the long waveguide shows less disturbing contributions of radiation transmitted through the cladding.

4. Conclusion

In conclusion, the present experiment verifies the results of field calculations and shows the energy range within which the waveguide may be applied to provide a small and coherent beam with sufficient intensity and low background. Furthermore, it clearly demonstrates that the electromagnetic field at the exit of a front-coupled planar waveguide and in the far-field may be very different from that expected behind a hypothetical slit of the same size.

We thank Ullrich Pietsch for providing beam time at the EDR beamline, as well as Wolfram Leiterberger and Yves Bodenthin for experimental support. We furthermore acknowledge funding by the German Federal Ministry of Education and Research (BMBF, project 05 KS4MGA/9).

References

Als-Nielsen, J. (2001). *Elements of Modern X-ray Physics.* New York: Wiley.
Bergemann, C., Keymeulen, H. & van der Veen, J. F. (2003). *Phys. Rev. Lett.* **91**, 204801.
Bongaerts, J. H. H., David, C., Drakopoulos, M., Zwanenburg, M. J., Wegdam, G. H., Lackner, T., Keymeulen, H. & van der Veen, J. F. (2002). *J. Synchrotron Rad.* **9**, 383–393.
Feng, Y. P., Sinha, S. K., Deckman, H. W., Hastings, J. B. & Siddons, D. P. (1993). *Phys. Rev. Lett.* **71**, 537–540.
Fuhse, C., Jarre, A., Ollinger, C., Seeger, J., Salditt, T. & Tucoulou, R. (2004). *Appl. Phys. Lett.* **85**, 1907–1909.
Fuhse, C. & Salditt, T. (2005). *Physica B*, **357**, 57–60.
Jark, S. D. F. W., Lagomarsino, S., Giannini, C., Caro, L. D., Cedola, A. & Müller, M. (2000). *Nature (London)*, **403**, 638–640.
Jarre, A., Fuhse, C., Ollinger, C., Seeger, J., Tucoulou, R. & Salditt, T. (2005). *Phys. Rev. Lett.* **94**, 074801.
Jarre, A., Salditt, T., Panzner, T., Pietsch, U. & Pfeiffer, F. (2004). *Appl. Phys. Lett.* **85**, 161–163.
Kopylov, Y. V., Popov, A. V. & Vinogradov, A. V. (1995). *Opt. Commun.* **118**, 619–636.
Lagomarsino, S., Cedola, A., Cloetens, P., Fonzo, S. D., Jark, W., Souillié, S. & Riekel, C. (1997). *Appl. Phys. Lett.* **71**, 2557–2559.
Marcuse, D. (1974). *Theory of Dielectric Optical Waveguides.* New York/London: Academic Press.
Panzner, T., Leitenberger, W., Grenzer, J., Bodenthin, Y., Geue, T., Pietsch, U. & Möhwald, H. (2003). *J. Phys. D*, **36**, A93–97.
Pfeiffer, F., David, C., Burghammer, M., Riekel, C. & Salditt, T. (2002). *Science*, **297**, 230–234.
Scarmozzino, R. & Osgood, R. M. (1991). *J. Opt. Soc. Am. A*, **8**, 724–731.
Spiller, E. & Segmüller, A. (1973). *Appl. Phys. Lett.* **24**, 60–61.
Yeh, C. (1990). *Handbook of Fiber Optics.* San Diego: Academic Press.
Zwanenburg, M. J., Peters, J. F., Bongaerts, J. H. H., de Vries, S. A., Abernathy, D. L. & van der Veen, J. F. (1999). *Phys. Rev. Lett.* **82**, 1696–1699.